Journal of Nepal Geological Society, 2022, Vol. 63, pp. 109–122
https://doi.org/10.3126/jngs.v63i01.50846

Characterization of large-scale landslides and their susceptibility evaluation in central Nepal Himalaya

Bikash Phuyal[1], Prem Bahadur Thapa[2,*], and Krishna Chandra Devkota[3]

[1]Central Department of Geology, Tribhuvan University, Kirtipur, Kathmandu, Nepal
[2]Department of Geology, Tri-Chandra Multiple Campus, Tribhuvan University, Kathmandu, Nepal
[3]Global Institute for Interdisciplinary Studies, Kathmandu, Nepal
Corresponding author's email: prem.thapa@trc.tu.edu.np

ABSTRACT

Large-scale landslides (LSL) are characterized by complex nature of failure mechanism, which depend on geological setting and associated factors of the area. The aim of this research is to identify the distribution pattern of LSL and all landslides in the central Nepal Himalaya and evaluation of their controlling factors. 7239 landslides were extracted from the study area by the interpretation of satellite imageries and field surveyed information. 28 landslides were classified as LSL and descriptive statistics were calculated. A comparative susceptibility assessment between all landslides and LSL was performed by frequency ratio model (FRM). Landslide susceptibility assessed from FRM was classified into five categories using the natural breaks method and adjustment from field evidences: very low, low, medium, high and very high. The very high, high and medium susceptibility classes comprised of 38.91%, 33.29%, 18.76% for all landslides and 39.51%, 29.65%, 20.98% for LSL. The result clearly indicated that the role of controlling factors varies differently depending upon the size of distributed landslides. To understand the significance of controlling factors for LSL, different potential cases were validated by success rates with area under the curve (AUC). The computed AUC in success rates for LSL is 65% and for overall landslides with similar controlling factors is 75%. The AUC values in different potential cases showed that the prime factors to control the LSL are geomorphology, rainfall, and geological structures.

Keywords: Large-scale landslide, controlling factors, landslide susceptibility, validation

Received: 29 March 2022 **Accepted:** 16 August 2022

INTRODUCTION

The complex geological nature and uneven fragile topography cause the landslides common in the Himalaya. Landslides are one of the most significant land degradation processes prevalent in the central Nepal Himalaya. This region is tectonically unstable with uneven topography, unstable geological structures, soft and fragile rocks, frequent earthquakes, along with heavy and prolonged precipitations during monsoon periods (Devkota et al., 2013; Nepal et al., 2019).

Landslides in the Himalaya are very common process of mass wasting and are scale dependent from small slope failures to massive extent of whole mountain collapse (Shroder and Bishop, 1998; Shang et al., 2003). Landslides often classified based on factors; materials, landslide scale, or type of movement (Varnes, 1978; Cruden and Varnes, 1996; Hungr et al., 2014). The size of landslide larger than 10^5 m^2 is commonly accepted to be large-scale landslides (Wen and Chen, 2007; Lin et al., 2013; Zhou and Cheng, 2015) and volume larger than 10^6 m^3 (Brueckl and Parotidis, 2001; Zerathe et al., 2014; Chung et al., 2018; Kuo et al., 2018).

The large-scale landslides (LSL) are characterized by complex nature of failure (Varnes, 1978; Wilson et al., 2003; Ghobadi et al., 2017; Kuo et al., 2018). The LSL is largely controlled by the geological setting of the area i.e. orientation of the rock strata with respect to slope (Timilsina et al., 2012; Chung et al., 2017; Ghobadi et al., 2017). Inter-bedding characteristics of rock strata with different mechanical property is another prime geological factor (Zerathe et al., 2014; Ghobadi et al., 2017; Zhou et al., 2019). The distribution pattern of LSL shows close relation to the seismic fault/thrust (Huang and Li, 2008, 2009) and most of the LSL are found to be oriented perpendicular to direction of the regional thrust system and proximity to the fault/thrust system (Timilsina et al., 2012; Zhou et al., 2019).

The effects of rainfall duration and cumulated rainfall are much more remarkable for LSL than for small landslides (Kuo et al., 2018). The major factors that affect the distribution of LSL triggered by the seismic event are distance effect, locked segment effect, hanging wall effect and direction effect (Xu et al., 2011). LSL triggered by the earthquake are to be concentrated in large seismic energy concentrated area due to energy released in these areas after rupture and displacement of the seismic fault. The majority of LSL are distributed on the hanging wall of the seismic fault and susceptible towards the slope facing to the travel direction of seismic wave as well as coincide with the staggering direction of the seismic fault (Xu et al., 2011). Timilsina et al. (2012) and Hasegawa et al. (2008) describe findings of the morphometric and geomorphic characteristics and its causes in Nepal Himalaya. The spatial distribution and failure characteristics can only be understandable after knowing the role and contribution of controlling factors. Therefore, the aim of this research is to identify the distribution pattern of LSL in central Nepal Himalaya and role of the controlling factors in terms of other smaller landslides converging to the LSL or isolated slides.

GEOLOGICAL SETTING

The central Nepal Himalaya is characterized by the complex geological and structural nature from Sub-Himalayan, Lesser Himalayan, Higher Himalayan and Tethys Himalayan tectonic divisions. Dhital (2015) described the rock sequences chronologically in the central Nepal Himalaya (Fig. 1). The Main Frontal Thrust (MFT) distinguishes the quaternary sediments of Terai from Sub-Himalayan rock strata (Middle Miocene to Early Pleistocene) mainly having sandstone, mudstone, conglomerate (Dhital, 2015). Similarly, the Main Boundary Thrust (MBT) separates the Sub-Himalayan rocks from Lesser Himalayan rocks (Paleoproterozoic to Neoproterozoic) and Main Central Thrust (MCT) separates the Lesser Himalayan rock from Higher Himalayan rocks (Stöcklin and Bhattarai, 1977; Stöcklin, 1980). The major tectonic structures are Midland Antiform, Great Mahabharat Synclinorium, Okhaladhunga Window and Kathmandu Nappe (Stöcklin and Bhattarai, 1977; Dhital, 2015). These structures resulted intense deformation within a rock stratum of the area, which can be one of the major reason to initiate and propagate the LSL.

METHODOLOGICAL APPROACH

The methodological approach have involved the acquisition of database, derivation of characteristics of landsides with respect to controlling parameters, evaluation of landslide susceptibility, validation and effect analysis (Fig. 2). The series of landslide data were collected during the study by the interpretation of satellite images, geological maps and geomorphic features. Field surveyed data were accompanied during the study to prepare the landslide database and inventory map. Landslides from the study area were extracted during the study and total 7239 landslides were mapped. Based on the size (e.g. Bruckl, 2001; Lin et al., 2013; Chung et al., 2018), 73 landslides are classified as large-scale landslides in the study area.

Database acquisition

A landslide inventory database is the vital information for landslide distribution and activity defined by Cruden and Varnes (1996) and WP/WLI (1993). Landslide inventory is the starting point for the landslide hazard or risk study to insight the spatial and temporal frequencies distribution in both space and time frame under international nomenclature (IAEG Commission on Landslides, 1990). A landslide inventory map is useful to establish the relationships between landslides and influencing factors as well as it is prerequisite to evaluate the landslide susceptibility (Chen et al., 2017).

The controlling factors of large-scale landslides (LSL) often defined by the geological condition, landslide scale (depth, area or volume), or type of movement. In Taiwan the current agreed-upon definition for a LSL is a landslide that is larger than 100,000 m^3 in volume (Brueckl and Parotidis, 2001; Zerathe et al., 2014; Chung et al., 2018). According to the Lin et al. (2013) the LSL are those having area larger than 10 ha (100,000 m^2). LSL can be clearly observed, the widened and flooded river channel filled by debris. As well as some researchers defined LSL based on its size (>100,000 m^2) (Wen and Chen, 2007; Zhou and Cheng, 2015) to make the inventory process easier.

The landslide spatial data were acquired by the interpretation of satellite images, geological maps and geomorphic features. Field surveyed data were accompanied during the study to verify the landslide database and inventory map. Spatial and attribute database of landslides were compiled and a total of 7239 landslides were depicted (Fig. 3). Based on the size, 73 landslides were initially classified as large-scale landslide

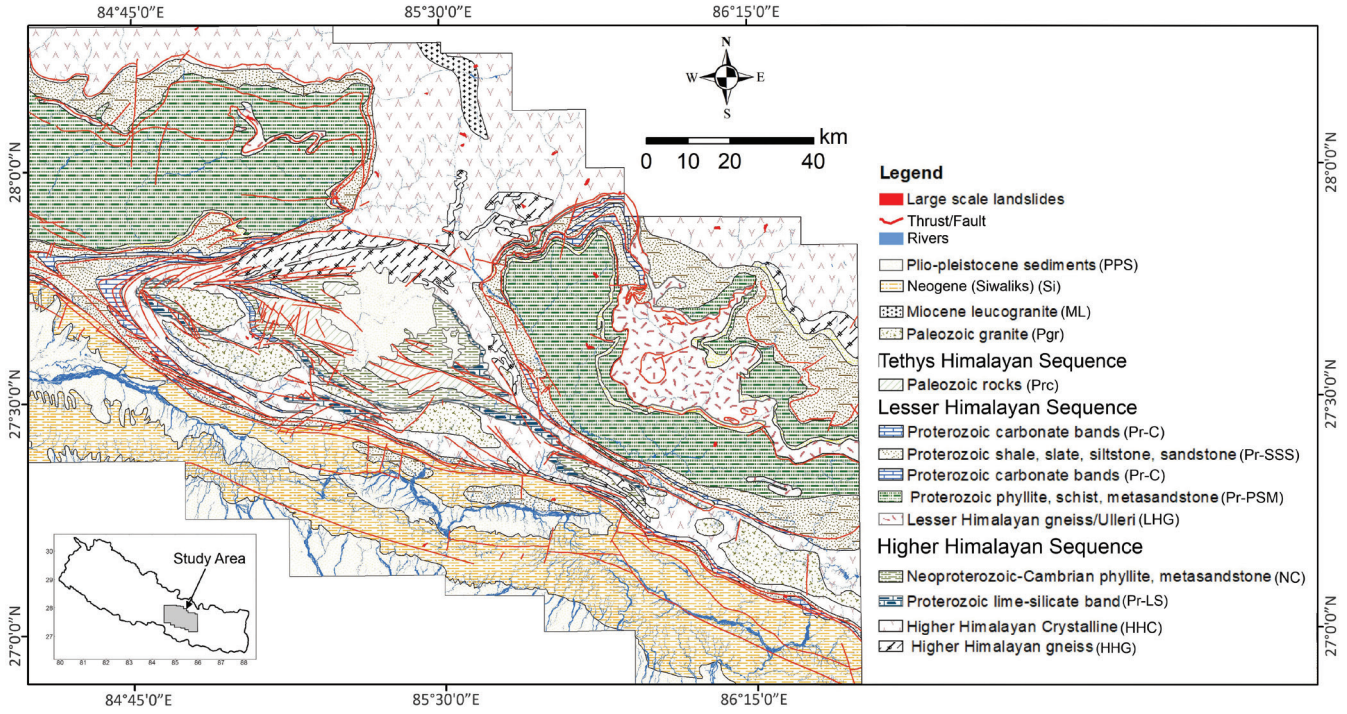

Fig. 1: Generalized geological map of the study area (modified after Dhital, 2015; DMG, 1980).

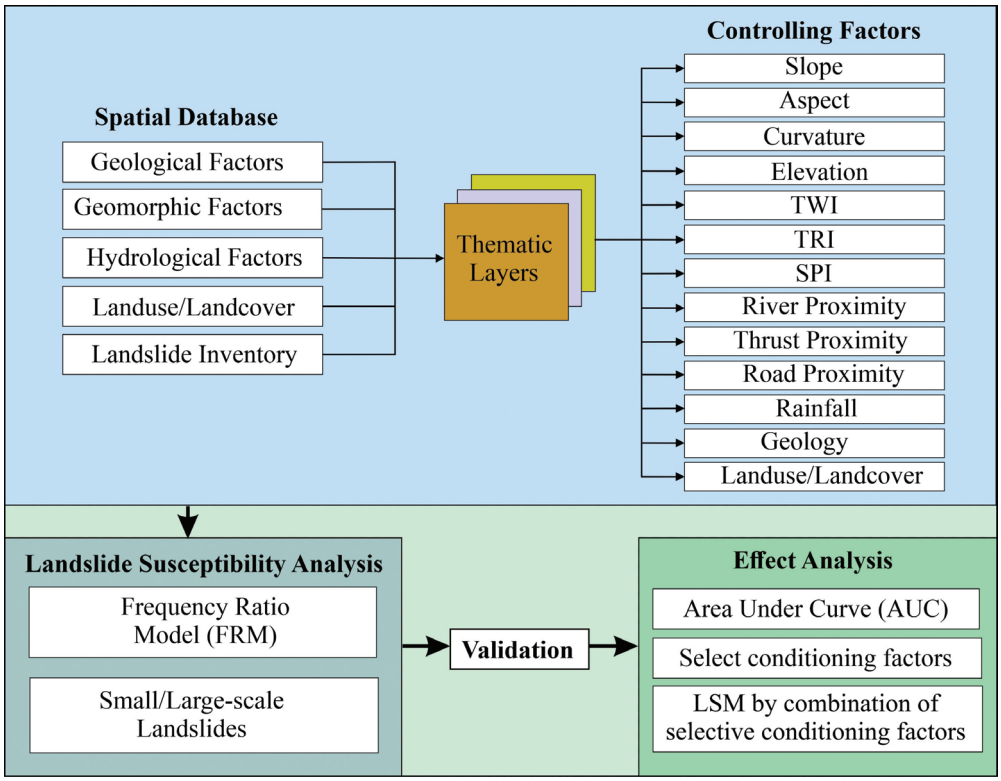

Fig. 2: Flowchart of methodological approach.

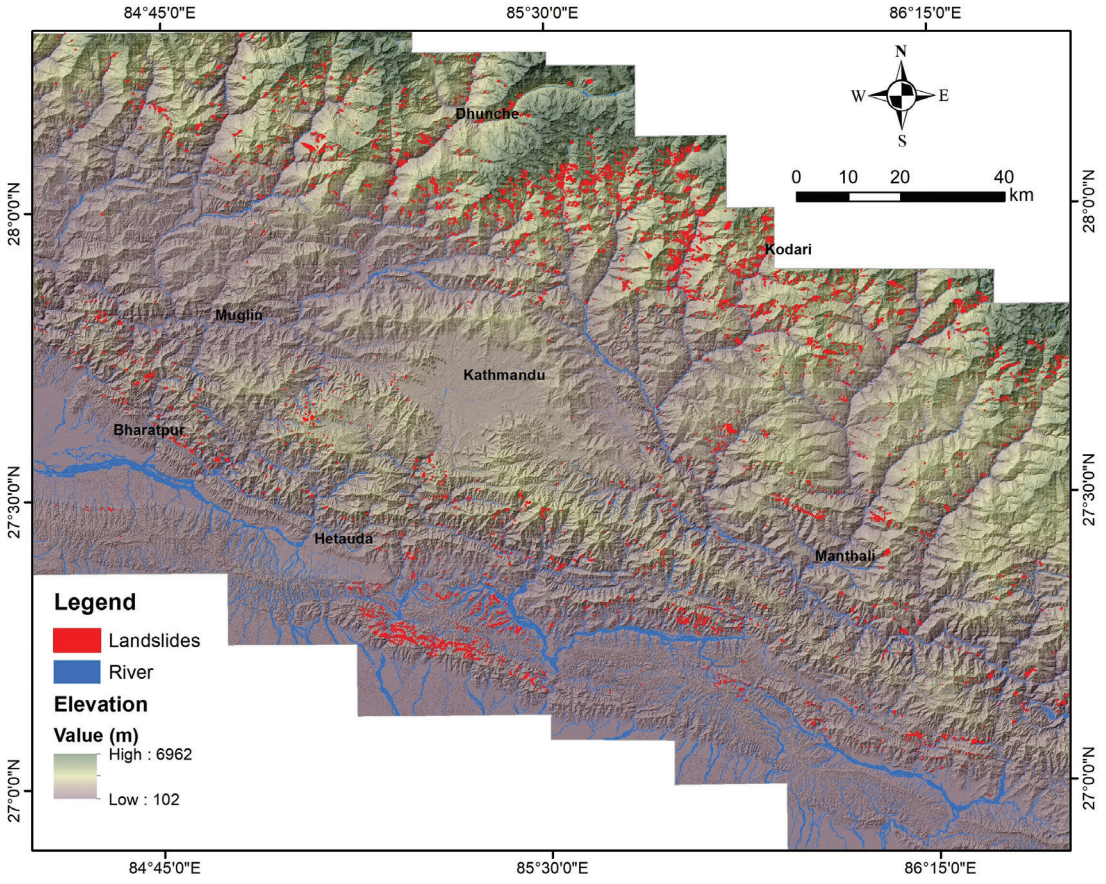

Fig. 3: Landslides inventory map of the central Nepal Himalaya.

(Bruckl, 2001; Lin et al., 2013; Chung et al., 2018). After considering the geological variation with associated structures and geometrical characteristics of slope and rock strata, 28 landslides were identified as LSL.

Spatial distribution pattern of LSL shows that majority of LSL (71%) having area less than 500,000 m^2, 25% of LSL have area range 500,000 to 1,000,000 m^2 and 4% of LSL have area size greater than 1,000,000 m^2 (Fig. 4). The average size of LSL is 356,706 m^2 that have mean length of 1125 m and width of 543 m.

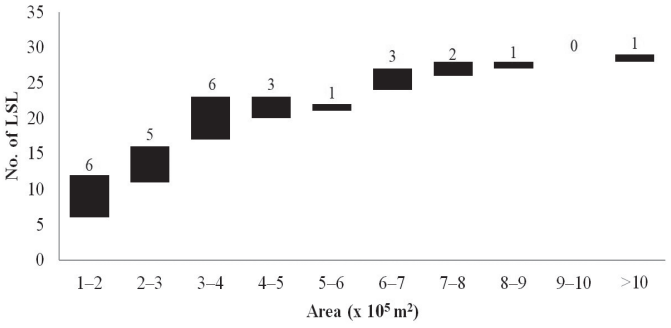

Fig. 4: Distribution pattern of large-scale landslides (LSL).

Controlling parameters

Reasonable classification of controlling factors helps to improve the reliability of landslide susceptibility mapping. Traditionally, it is done by extracting ridge lines and valley lines from high-resolution digital terrain models (DTM). It divides watersheds into separate slopes based on hydrological analysis (Giles and Franklin, 1998; Guzzetti et al., 1999). Based on the geological environment and landslide distribution pattern, a total of thirteen landslide conditioning factors were considered during the landslide susceptibility mapping: elevation, slope angle, slope aspect, curvature, stream power index (SPI), topographic roughness index (TRI), topographic wetness index (TWI), distance to road, distance to river, distance to thrust, rainfall, lithology, and land cover (Fig. 5).

Slope angle is widely used in landslide susceptibility evaluation and is also an important factor when evaluating slope stability. The possibility of landslide occurrence increases with increasing slope angle (Demir et al., 2013). Slope angles in the study area are divided into five classes: <15°, 15–25°, 25–35°, 35–45°, and >45° (Fig. 5a).

Slope aspect refers to variation in the intensity of sunlight received, which affects soil moisture, evaporation and erosion. These factors influence the development of landslides (Ilia and Tsangaratos, 2016). In the study area, slope aspect is divided into nine classes: flat, north, northeast, east, southeast, south, southwest, west and northwest as shown in Figure 5b. Distance from river, affects the concentration of landslides, shows inverse relationship. In this study distance to rivers is classified as <20 m, 20–40 m and >40 m (Fig. 5c).

The curvature map in the study area is sub-classified in to three class; concave, flat and convex (Fig 5d). Elevation is considered a vital factor that influences the occurrence and distribution of landslides, degree of weathering and human activities (Hong et al., 2016). In the study area, the elevation values are divided into four classes: <1000 m, 1000–2000 m, 2000–3000 m, 3000–4000 m and >4000 m (Fig. 5e). Similarly, the area is separated based on the proximity to road and divided into <25 m, 25–50 m, >50 m sub-classes (Fig. 5f).

TRI express the amount of elevation difference between adjacent cells of a DEM developed by Riley et al. (1999). In present study, TRI values divided into three classes as; <0.3, 0.3–0.6, and >0.6 (Fig. 5g). SPI is useful to describe potential flow erosion at the given point of the topographic surface (Moore et al., 1991). Three sub-classes; <50, 50–100, and >100 is categorized to describe the SPI classes in this study (Fig. 5h). The proximity to thrust is classified into >50 m and <500 m, 500–1000 m and >1000 m are shown in Figure 5i. The TWI is a useful model to estimate where water will accumulate in an area with elevation differences. It is a function of slope and the upstream contribution area. Three classes are categorized for this DEM derivatives; <4, 4–6, and >6 (Fig. 5j).

Annual rainfall is important triggering factor of landslide. Chalise and Khanal (2001) established 1500–2500 mm mean annual rainfall are predominates over most of the country. It is taken as important triggering factor and is classified as <1200 mm, 1200–1400 mm, 1400–1600 mm, 1600–1800 mm, >1800 mm sub-classes (Fig. 5k). Land cover pattern also play significant role to produce the landslides. The land cover map of the study area is categorized as barren land, buildings, bush, cliff, cultivation, forest, glacier, grass, lake, river, sand, snow and swamp (Fig. 5l). Lithology is an important factor in the formation and evolution of landslides, as it forms the material base for landslide generation (Yalcin et al., 2011). Slopes formed by different rock and soil masses have different physio-mechanical properties (Pellicani et al., 2014). There are fourteen lithological units in the study area.

The landslide controlling thematic layers were used subsequently to derive the landslides characteristics, susceptibility evaluation and validation of analysis. Descriptive statistics values for different LSL controlling parameters is presented in the Table 1.

Table 1: Descriptive statistics of landslide controlling factors.

Controlling Variables	Statistical values			
	Min.	Max.	Mean	Std. dev.
Landslide area	102459.6	1020250	356706.5	239464.8
Landslide length	457	2186	1125.86	511.27
Landslide width	257	1277	543.96	244.69
Slope angle	0	86.21	27.64	14.64
Slope aspect	-1	359.9	178.63	103.21
Curvature	-655	1095	0	8.81
Elevation	102	6962	1476.02	1101.58
TRI	0.01	0.99	0.5	0.09
SPI	0	2222558	234.04	2576.69
TWI	-0.38	20.89	4.6	1.83
Distance to river	0	8761.47	1443.17	1459.26
Distance to road	0	30104.72	5262.04	4883.97
Distance to thrust	0	33966.17	4185.28	5070.96
Rainfall	1076.09	2185.62	1591.46	152.73

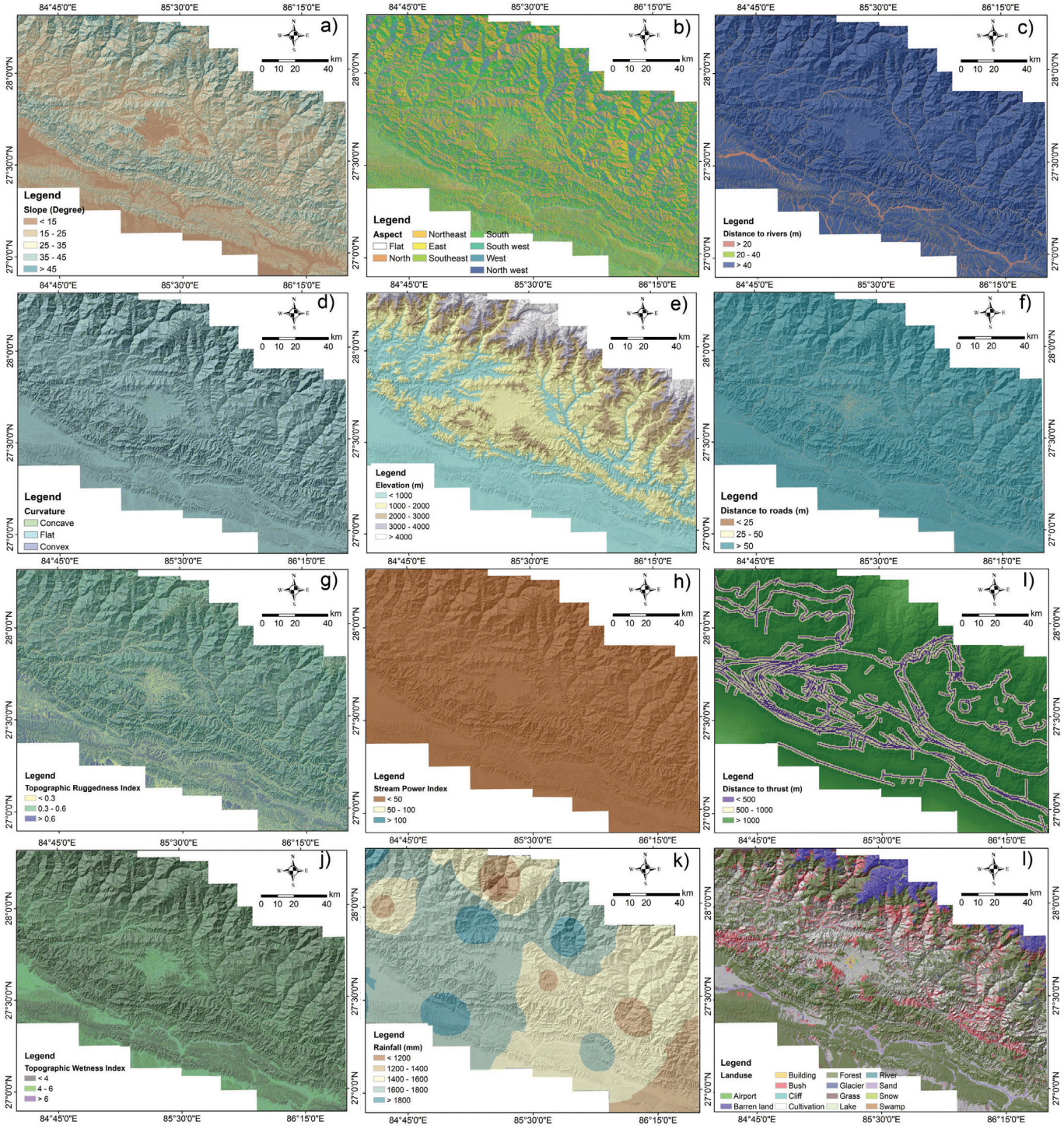

Fig. 5: Thematic layers; a) Slope angle, b) Slope aspect, c) Distance to river, d) Curvature, e) Elevation, f) Distance to road, g) TRI, h) SPI, i) Distance to thrust, j) TWI, k) Rainfall, l) Land cover.

Assessment methods

The theoretical concepts of assessment method include the univariate analysis for distribution pattern and landslide characteristics. Bivariate approach has evaluated the landslide susceptibility and validation of results. The landslide susceptibility assessment is based on the influences of controlling factors over the spatial distribution of landslides and the prediction of landslide events will occur under the same physio-mechanical environment of the past events (Lee and Talib, 2005). The relationship between spatial distribution and controlling factors to distinguish the degree of susceptible zone, landslide susceptibility mapping is usually done using soft computing-based techniques and geographic information system (Cardenas and Mera, 2016). The deterministic models for the susceptibility assessment are based on mathematical

relations that depends on the physical laws of resisting and driving forces acting on a slope masses. The statistical models are data driven method that possess the inaccuracy in the input data may cause a significance error in the results. Thus, it requires the complete inventory dataset for the assessment and model validation (Van Westen et al, 2008; Trigila et al., 2015).

The FRM is used in this study, based on the spatial relationships between all landslides and each landslide conditioning factor, is a simple probabilistic model that is widely used in landslide susceptibility mapping (Choi et al., 2012; Mohammady et al., 2012). This quantitative approach for landslide susceptibility is examined using GIS techniques and spatial data (Lee and Talib, 2005; Reis et al., 2012; Umer et al., 2014; Chen et al., 2016; Ding et al., 2017, Wang and Li, 2017). The frequency ratio (FR) is the ratio of landslide areas to the total study area and is also the ratio of landslide occurrence probability to non-occurrence for a given attribute. If the ratio is >1, it indicates a higher correlation and if the ratio is <1 there is a lower correlation. The value of FR (Mondal and Maiti, 2013; Youssef et al., 2015) is expressed as Equation 1.

$$FR = \frac{Mi/M}{Ni/N} \quad (1)$$

where, *Mi* is the number of pixels with landslides for each subclass conditioning factor, *M* is the total number of landslides in the study area, *Ni* is the number of pixels in the subclass area of each factor and *N* is the number of total pixels in the study area.

In this study, normalized frequency ratio method used to deliver the output. The calculation is followed to normalization of each derived FR value to discretize the continuous factor values from 0 to 1 range. In arrange to discover the relative significance of each spatial factor with the accessible preparing dataset; the prediction rate (PR) was analyzed depending upon its degree of spatial affiliation with the preparing datasets (Eq. 2) (Baral et al., 2021).

$$PR = \frac{RFmax - RFmin}{(RFmax - RFmin)min} \quad (2)$$

where, *RFmax* and *RFmin* is the maximum and minimum relative frequency among the classes within a factor, *(RFmax–RFmin)min* is the is the minimum values among all the factors considered.

Essential component of the landslide assessment is the validation of analysis results that can be used for the prediction of landslides with areas having similar controlling factors (Gorsevski et al., 2000; Lee at al., 2004; Chung and Fabbri, 2003; Wubalem, 2021). The validation of the landslide susceptibility generally follows the calculation of the success and prediction rates. The success of the model is based on known landslide events whereas the prediction rate fits with landslides which are not incorpoted in the model evaluation (Chung and Fabbri, 1999) and many authors have addressed their corresponding issues of the result validation (Carrara et al., 1991; Chung et al., 1995; Luzi and Pergalani, 1996; Chung and Fabbri, 2003; Dymond et al., 2006; Meusburger and Alewell, 2009; Wahono, 2010). The calculated results were plotted in percentage that classified as susceptible (*x*-axis) versus the cumulative percent of landslide occurrence (*y*-axis), with the area under the curve (AUC) calculation from Equation 3 (Pimiento, 2010).

$$AUC = \sum_{i=0}^{n} (x_i - x_{i-1}) y_i - \left[\frac{(x_i - x_{i-1})(y_i - y_{i-1})}{2}\right] \quad (3)$$

The AUC measures the accuracy of results in the assessment landslide susceptibility (e.g. Chung, and Fabbri, 2003; Pimiento, 2010, Fleuchaus et al., 2021). The values of AUC is between a maximum value of 1 or equal to 100% and 0.5 or equal to 50%. Different ranges of AUC can be classified for the prediction models (0.9 as a very good, 0.8–0.9 as a good, 0.7–0.8 as a medium or reasonable, and <0.6 poor) i.e. the higher the AUC value of an influencing factor, the higher the influence of the landslide event (Silalahi et al., 2019).

RESULT AND DISCUSSION

Based on the spatial and attribute databases of landslides and their controlling parameter, distribution pattern and characteristics of landslides were derived. Frequency ratio model was implemented to evaluate landslide susceptibility. The susceptibility models were validated by computing success rates and the influence of various controlling parameters were evaluated by adjusting parameter combinations in effect analysis.

Distribution pattern and characterization

The distribution pattern of landslides in the central Nepal Himalaya is influenced by the role of controlling factors (Hasegawa et al., 2008; Timilsina et al., 2012). Slope is the prime geomorphometric factor to influence the landslide patterns in the region. The study has shown that slope angle map has a significant impact on the distribution of landslides. The landslides occurrence rate is increased with increasing slope angles. The higher landslide frequency at the slope angle 25°–45°. The lower landslide frequency at the low slope angle (<25°) is due to less driving force acting on gentle slope. The presence of cliffs at high slope angle area is another reason to be less prone for the landslide events. Study showed higher the gradient high FR and greater than one for slope angle greater than 25°. The highest FR is 2.5±0.28 for the slope angle greater than 45°. The FR exceed one at southeast, south and southwest facing slopes (Table 2) that represent the landslides are more likely on these slopes. Conversely, FR values of the remaining slope aspect categories are lesser than one, indicating low probability of landslide occurrences. The concave slope curvature has high landslides distribution with FR 1.09±0.03. The elevation range showed distinct landslide distribution patter. The distribution of landslides is high in the elevation range 1000–3000 m with maximum obtained FR is 3.7±0.38 showing a positive correlation with landslide occurrence.

The most significant landslide triggering factor is rainfall which is more remarkable for LSL distribution (Kuo et al., 2018). In the area, rainfall 1600–1800 mm presented higher number of landslide distribution and the calculated FR for same rainfall class is 1.12±0.1, suggest that such rainfall class area is prone to trigger the landslide. In the area, the geological units; Higher Himalayan Crystalline, Lesser Himalayan Gneiss, Proterozoic

carbonate rocks, Paleozoic rocks and Miocene leuco-granite have high landslide frequency and the FR is significant (>1). This indicates that these geological classes are prone to the LSL due to variable mechanical properties of inter-bedding characteristics and geometric orientation of rock strata (Wilson et al., 2003; Timilsina et al., 2012; Zerathe et al., 2014; Chung et al., 2017; Ghobadi et al., 2017; Kuo et al., 2018). The land cover types; barren land, bush/grass land and forest, which represents to high landslide distribution with some of significant FR (>1) is shown in Table 2.

The spatial distribution of the landslides in the Himalayan terrain is significantly influenced by the fault/thrust systems. The distribution of landslides in the proximity to the thrust is appreciably high in case of LSL than all landslides (Table 2). It clearly showed seismic fault/thrust has a close relation to the LSL distribution pattern (Huang and Li, 2008, 2009; Xu et al, 2011; Zhou et al., 2019). Also, the orientational direction of LSL are mostly perpendicular with the regional fault/thrust system (Xu et al., 2011). The proximity to road and river also indicated certain distribution patterns of landslides in the vicinity of 40-50 m (Table 2).

This study focused on the characterization of LSL after knowing its distribution pattern in the central Nepal by establishing the relationship between the LSL and its controlling factors.

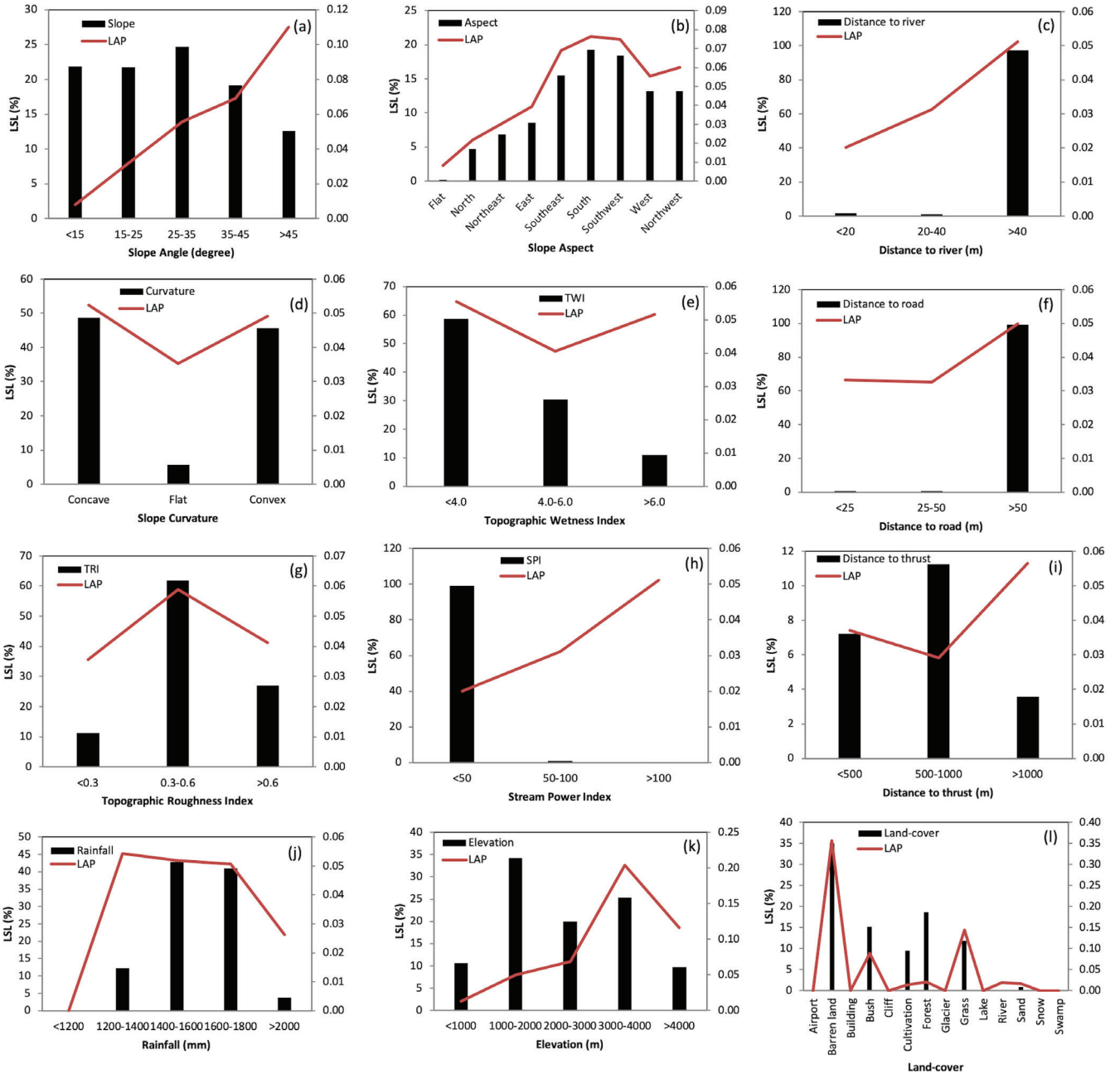

Fig. 6: Controlling factors of LSL and their frequency distribution; (a) Slope angle, (b) Slope aspect, (c) Distance to river, (d) Slope curvature, (e) Topographic wetness index, (f) Distance to road, (g) Topographic roughness index, (h) Stream power index, (i) Distance to thrust, (j) Rainfall, (k) Elevation, (l) Land-cover.

Geomorphometric, geological, hydrogeological and landcover/ land-use practice are major factors associated with the LSL (Huang and Li, 2008; Timilsina et al., 2012; Ghobadi et al., 2017). Slope is the prime factor to define the dimension of the landslides and in the region study area ranges from 0° to 86.21° slope angle which is divided into 5 intervals. The pixel count of LSL in the interval greater than 45° is largest (28.04%) and followed by interval 25°–35° i.e. 27.84%. The landslide area percentage (LAP) plot reached their peak 0.11% at class interval of greater than 45°. The result shows that higher the slope then more likely LSL is to occur (Fig. 6a). The slope angle class 25°–45° is found to be sensitive for the LSL due to vertical and lateral thickness of slope forming materials in this slope angle range (Li et al., 2022). The slope aspect is categorized to 9 classes from -1 to 359.9. The large number of LSL falls on south aspect (19.28%) and the LAP reached its peak (0.08%) at the same class of slope aspect (Fig. 6b). The most of LSL (97.4%) falls at greater than 40 m distance to river and peak LAP (0.05%) at same class (Fig. 6c). Similarly, curvature of the area ranges from -655 to 1095. The concave slope has large number of LSL (48.73%) and in the same class of curvature LAP has its peak value (0.05%) (Fig. 6d). The large number of LSL are present in classes as less than 4 by 58.65% and LAP reached their peak 0.06% at less than 4 (Fig. 6e). 99.06% of LSL are present at less than 50 m distance to road and peak LAP value is 0.05% for same distance to roads classes (Fig. 6f). The classes of TRI and SPI categorized to 3 classes. The large number of LSL are present in classes as 0.3 to 0.6 by 61.82% (Fig. 6g) and less than 50 by 98.99% (Fig. 6h) for TRI and SPI respectively. The LAP for same factors reached their peak 0.06% at 0.3 to 0.6 and 0.36% at greater than 100 accordingly. Likewise, most of LSL (81.54%) falls at greater than 1000 m distance to thrust and higher value of LAP belongs to same class having value 0.06% (Fig. 6i).

The rainfall of the study area ranged from 1076 to 2185 mm and is divided into 5 intervals in this work. The pixel count of LSL in the interval 1400–1600 mm is largest (42.91%) and followed by interval 1600–1800 mm i.e. 40.98%. LAP plot also reaches their peak 0.05% at class interval of 1400–1600 mm (Fig. 6j). The elevation of the study area ranges from 102 to 6963 m, divided at 1000 m intervals in this work. Statistics show that most of the LSL (34.27%) are located at elevations from 1000 to 2000 m. The peak value of LAP is 0.2% at 3000 to 4000 m (Fig. 6k). Lithological unit from study area i.e. Higher Himalayan Crystalline has large number of LSL (49.91%) and the LAP value is higher (0.2%) for Miocene Leucogranite. This indicates the lithological classes are highly prone to LSL. The influence of land cover types on the occurrence of landslides is also obvious. Among the classes, barren land has large number of LSL present (34.94%) and the LAP reaches the peak 0.36% for same class, implying LSL prone area (Fig. 6l).

Susceptibility zonation

Using frequency ratio model (FRM), the susceptibility zonation were carried out by utilizing two different spatial sets of landslides. Many researchers in the Himalayan terrain (e.g. Devkota et al., 2012; Regmi et al., 2012; Thapa, 2011; Pathak, 2016) used the FRM and combinations of similar parameters for the landslide susceptibility assessment. The comparison was performed between the all landslides and large-scale landslides to characterize the influence of controlling parameters for susceptibility zonation.

The landslide susceptibility Index (LSI) map based on the distribution of all slides was derived using FR model from the selected controlling factors classes were processed in GIS. The LSI map is reclassified into five categories via natural breaks method; very low, low, medium, high and very high (Fig. 7a). Each of these categories covers 13.79%, 28.76%, 29.28%, 20.06% and 8.11% of the total area of the region, respectively. The very high, high and medium areas contain 38.91%, 33.29% and 18.76% of the total of all landslides, respectively; while the low and very low areas contain only 7.37% and 1.66% of the total landslides, respectively.

The LSI map from the distribution of the LSL also obtained using FR values which was divided into five categories using the natural breaks method: very low, low, medium, high and very high (Fig. 7b). Each of these categories covers 8.09%, 23.06%, 32.07%, 25.94% and 10.84% of the total area of the region, respectively. The very high, high and medium areas

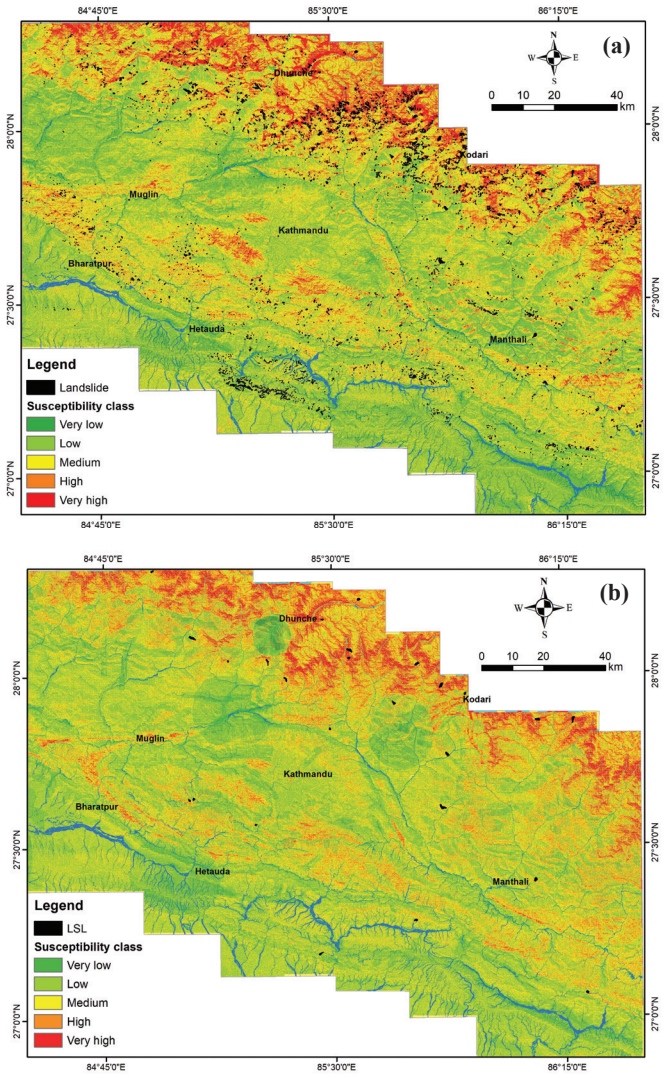

Fig. 7: Landslide susceptibility maps based on datasets: (a) All landslides, (b) Large-scale landslides.

Table 2: The relationship between landslides and their controlling parameters.

	Category	Class pixel	Class (%)	landslide (%)		FR		Normalized FR		RF		Min RF (a)		Max RF (b)		(c)		(d)		PR (c/d)	
				All	LSL	All	LSL	All	LSL	All	LSL	All	LSL	All	LSL	All	LSL	All	LSL	All	LSL
Slope angle	< 15	50113449	21.82	3.17	3.45	0.15	0.16	0.05	0.07	0.03	0.03	0.03	0.03	0.47	0.40	0.44	0.37	0.05	0.09	9.17	4.24
	15-25	49912164	21.73	9.27	14.01	0.43	0.64	0.16	0.29	0.07	0.12										
	25-35	56778650	24.72	23.21	27.84	0.94	1.13	0.34	0.51	0.16	0.20										
	35-45	43922932	19.12	29.93	26.67	1.57	1.39	0.57	0.63	0.27	0.25										
	> 45	28992529	12.62	34.41	28.04	2.73	2.22	1.00	1.00	0.47	0.40										
Slope aspect	Flat	2686515	1.17	0.10	0.18	0.09	0.15	0.04	0.11	0.01	0.02	0.01	0.02	0.26	0.18	0.25	0.16	0.02	0.03	13.26	4.99
	North	26708566	11.63	2.72	4.73	0.23	0.41	0.11	0.29	0.03	0.05										
	Northeast	27665527	12.04	5.04	6.85	0.42	0.57	0.20	0.40	0.05	0.07										
	East	26984496	11.75	11.48	8.61	0.98	0.73	0.48	0.51	0.12	0.09										
	Southeast	27742176	12.08	21.99	15.52	1.82	1.29	0.89	0.90	0.23	0.16										
	South	31116252	13.55	27.84	19.28	2.06	1.42	1.00	1.00	0.26	0.18										
	Southwest	30416122	13.24	19.64	18.44	1.48	1.39	0.72	0.98	0.19	0.17										
	West	29334657	12.77	8.24	13.20	0.64	1.03	0.31	0.73	0.08	0.13										
	Northwest	27065413	11.78	2.94	13.20	0.25	1.12	0.12	0.79	0.03	0.14										
Geology	PPS	21720483	9.46	0.63	0.00	0.07	0.00	0.03	0.00	0.01	0.00	0.01	0.00	0.17	0.31	0.17	0.31	0.01	0.01	23.92	30.15
	HHG	7041705	3.07	2.41	3.84	0.79	1.25	0.35	0.30	0.06	0.09										
	Pr-PSM	3152383	1.37	0.59	1.06	0.43	0.77	0.19	0.19	0.03	0.06										
	Pr-PSM	44051911	19.18	17.19	25.27	0.90	1.32	0.40	0.32	0.07	0.10										
	Pr-Qz	3261885	1.42	1.13	0.00	0.79	0.00	0.36	0.00	0.06	0.00										
	Pr-SSS	26910257	11.71	9.79	1.60	0.84	0.14	0.37	0.03	0.07	0.01										
	HHC	51572289	22.45	50.03	49.91	2.23	2.22	1.00	0.54	0.17	0.16										
	LHG	9800321	4.27	5.16	6.85	1.21	1.61	0.54	0.39	0.09	0.12										
	ML	1109454	0.48	0.73	1.99	1.51	4.12	0.68	1.00	0.12	0.31										
	NC	5620748	2.45	0.96	1.15	0.39	0.47	0.18	0.11	0.03	0.03										
	PGr	8713719	3.79	0.60	0.00	0.16	0.00	0.07	0.00	0.01	0.00										
	PRc	3405613	1.48	2.05	0.39	1.38	0.26	0.62	0.06	0.11	0.02										
	Pr-C	4508567	1.96	3.40	1.91	1.73	0.97	0.78	0.24	0.14	0.07										
	Si	38850493	16.91	5.33	6.04	0.31	0.36	0.14	0.09	0.02	0.03										
Curvature	Concave	105875260	46.09	51.39	48.73	1.12	1.06	0.99	1.00	0.43	0.38	0.13	0.26	0.44	0.38	0.31	0.12	0.30	0.10	1.01	1.24
	Flat	34665492	15.09	5.08	5.59	0.34	0.71	0.30	0.68	0.13	0.26										
	Convex	89178972	38.82	43.53	45.68	1.12	0.99	1.00	0.94	0.44	0.36										
TWI	< 4	120441741	52.43	56.66	58.68	1.08	1.12	0.92	1.00	0.35	0.38	0.27	0.28	0.38	0.38	0.11	0.10	0.08	0.07	1.39	1.35
	4--6	85281141	37.12	31.05	30.44	0.84	0.82	0.71	0.73	0.27	0.28										
	> 6	23996842	10.45	12.29	10.87	1.18	1.04	1.00	0.93	0.38	0.35										
TRI	< 0.3	35927596	15.64	14.25	11.24	0.91	0.72	0.77	0.61	0.32	0.26	0.26	0.26	0.42	0.43	0.15	0.17	0.06	0.04	2.65	4.15
	0.3 - 0.6	119687189	52.10	61.58	61.82	1.18	1.19	1.00	1.00	0.42	0.43										
	> 0.6	74400263	32.39	24.18	26.94	0.75	0.83	0.63	0.70	0.26	0.30										

	Category	Class pixel	Class (%)	landslide (%)		FR		Normalized FR		RF		Min RF (a)		Max RF (b)		(c)		(d)		PR (c/d)	
				All	LSL	All	LSL	All	LSL	All	LSL	All	LSL	All	LSL	All	LSL	All	LSL	All	LSL
SPI	< 50	229269939	99.80	98.78	98.99	0.99	0.99	0.07	0.14	0.05	0.07	0.05	0.07	0.66	0.55	0.61	0.47	0.24	0.31	2.54	1.55
	50 - 100	434316	0.19	1.13	0.96	5.98	5.08	0.44	0.69	0.29	0.38										
	> 100	15469	0.01	0.09	0.05	13.69	7.31	1.00	1.00	0.66	0.55										
Distance to river	< 20	9362916	4.08	2.99	1.65	0.73	0.41	0.72	0.39	0.27	0.20	0.27	0.20	0.38	0.50	0.10	0.30	0.08	0.11	1.29	2.79
	20-40	3442770	1.50	1.42	0.94	0.95	0.63	0.94	0.61	0.35	0.30										
	> 40	216912196	94.42	95.59	97.40	1.01	1.03	1.00	1.00	0.38	0.50										
Distance to road	< 25	1689570	0.74	0.29	0.49	0.39	0.67	0.39	0.67	0.22	0.29	0.21	0.28	0.57	0.43	0.36	0.15	0.01	0.01	40.65	25.29
	25-50	1580527	0.69	0.26	0.45	0.37	0.66	0.37	0.65	0.21	0.28										
	> 50	226393668	98.55	99.46	99.06	1.01	1.00	1.00	1.00	0.57	0.43										
Rainfall	<1200	1278051	0.56	1.04	0.00	1.86	0.00	1.00	0.00	0.34	0.00	0.12	0.00	0.34	0.30	0.22	0.30	0.03	0.14	6.47	2.07
	1200-1400	25743799	11.21	9.32	12.27	0.83	1.10	0.45	1.00	0.15	0.30										
	1400-1600	93948522	40.90	36.17	42.91	0.88	1.05	0.47	0.96	0.16	0.28										
	1600-1800	92123221	40.10	48.80	40.98	1.22	1.02	0.65	0.93	0.22	0.28										
	>2000	16669267	7.26	4.67	3.84	0.64	0.53	0.35	0.48	0.12	0.14										
Land cover	Airport	17922	0.01	0.00	0.00	0.00	0.00	0.00	0.00	0.00	0.00	0.00	0.00	0.35	0.54	0.35	0.54	0.03	0.02	13.03	25.32
	Barren land	11165719	4.86	17.67	34.94	3.63	7.19	1.00	1.00	0.31	0.54										
	Building	250288	0.11	0.00	0.00	0.00	0.00	0.00	0.00	0.00	0.00										
	Bush	19410676	8.45	9.91	15.15	1.17	1.79	0.32	0.25	0.10	0.14										
	Cliff	276950	0.12	0.00	8.92	0.00	73.96	0.00	0.00	0.00	0.00										
	Cultivation	76648928	33.38	10.30	9.47	0.31	0.28	0.08	0.04	0.03	0.02										
	Forest	105174575	45.80	37.98	18.67	0.83	0.41	0.23	0.06	0.07	0.03										
	Glacier	199636	0.09	0.00	0.00	0.00	0.00	0.00	0.00	0.00	0.00										
	Grass	9414794	4.10	16.49	11.86	4.02	2.89	1.11	0.40	0.35	0.22										
	Lake	46833	0.02	0.00	0.00	0.00	0.00	0.00	0.00	0.00	0.00										
	River	1007729	0.44	0.19	0.17	0.42	0.39	0.12	0.05	0.04	0.03										
	Sand	5858477	2.55	1.75	0.82	0.69	0.32	0.19	0.04	0.06	0.02										
	Snow	98568	0.04	0.00	0.00	0.00	0.00	0.00	0.00	0.00	0.00										
	Swamp	99	0.00	0.00	0.00	0.00	0.00	0.00	0.00	0.00	0.00										
Distance to thrust	< 500	22169579	9.64	7.86	7.22	0.82	0.75	0.76	1.00	0.30	0.44	0.30	0.21	0.39	0.44	0.09	0.23	0.01	0.13	9.36	1.72
	500-1000	43970164	19.11	16.11	11.24	0.84	0.59	0.79	0.79	0.31	0.35										
	> 1000	163911973	71.25	76.03	3.58	1.07	0.36	1.00	0.49	0.39	0.21										
Elevation	<1000	94217298	41.01	14.00	10.64	0.34	0.26	0.10	0.06	0.04	0.03	0.04	0.03	0.44	0.45	0.39	0.42	0.08	0.08	5.13	5.19
	1000-2000	78549425	34.19	31.80	34.27	0.93	1.00	0.28	0.24	0.12	0.11										
	2000-3000	33174501	14.44	29.17	19.91	2.02	1.38	0.60	0.34	0.26	0.15										
	3000-4000	14183533	6.17	20.76	25.39	3.36	4.11	1.00	1.00	0.44	0.45										
	>4000	9594967	4.18	4.28	9.78	1.02	2.34	0.30	0.57	0.13	0.26										

contain 39.51%, 29.65% and 20.98% of the LSL, respectively; while the low and very low areas contain only 8.12% and 1.73% of the total LSL, respectively (Fig. 8).

Analysis of landslide controlling factors for landslides and LSL showed the differential influence, which were assessed based on the frequency ratio (FR) values. The combination of DEM derivatives with the geology, rainfall, and land cover were utilized landslide susceptibility evaluation. The majority of landslides are found to be occurred in the areas of highly susceptible zones that verified the effectiveness of the landslide susceptibility mapping (Chen et al., 2017). 73% and 69% of small and large-scale landslides of this study are located in very high and high susceptibility classes. This result clearly indicated that significance of controlling factors for both all and large-scale landslides are different.

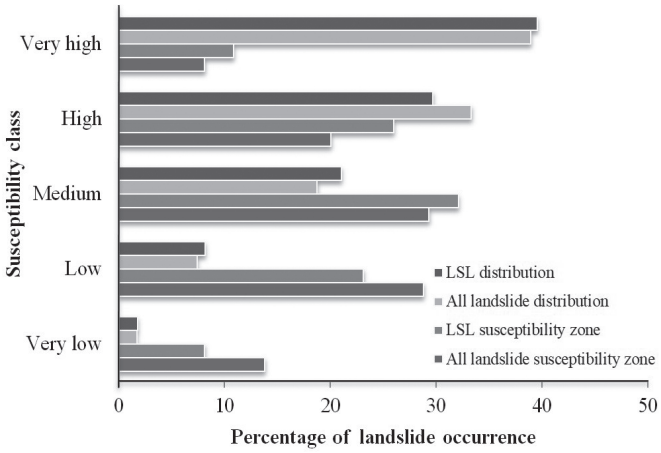

Fig. 8: Distribution of landslides in predicted landslide susceptibility classes.

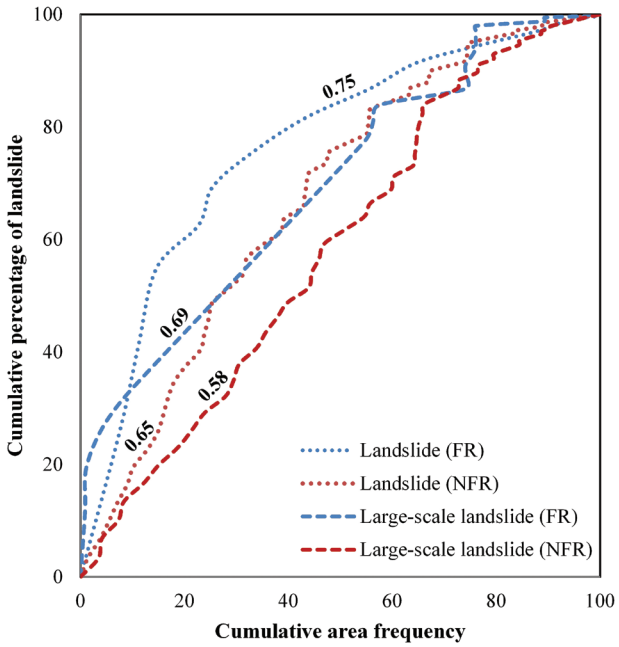

Fig. 9: Validation of landslide susceptibility assessment by success rates.

Validation and effect analysis

In the present study the AUC value for the success rate were determined and was checked in the field for the cross verification. The observation shows that area of high susceptible zone have significant presence of slope instability phenomena marked by landslide events. From the validation process, the AUC value of the success rate is 0.67 for all landslides and 0.58 for the LSL while picking the same controlling factors to the landslide events using normalized frequency ratio (NFR) values. However, the same quantitative validation results of AUC value for the all landslides is 0.75 and for LSL is 0.69 from the FR model. The result showed satisfactory aggrement between landslide susceptibility map and the prior landslide events. The AUC analysis (Fig. 9) shows that the results (success rate) of the susceptibility are more reliable for the all mapped landslides than LSL in both NFR and FR models in validation process.

Factor effect analysis is conducted by various researchers to evaluate the effects of controlling factors by adjusting input parameters (e.g. Lee and Talib, 2005; Pradhan and Lee, 2010). In this study, the accuracy assessment results of LSL showed the model accuracy by calculating success rates in terms of different combination of factors which is shown in Figure 10. The success rate calculated based on nine factors (slope, aspect, curvature, elevation, rainfall, geology, distance to thrust, distance to river, distance to road), the AUC is 0.65 i.e. accuracy of 65% (case I). In the case II, seven controlling factors were taken and AUC is found to be 0.69 (69% accuracy). Similarly, when six controlling factors for LSL were used (slope, aspect, curvature, rainfall, geology, distance to thrust), the AUC shows that the result of the susceptibility obtained from the FR model is the accuracy of 74% (case III). The better prediction of 79% accuracy model is accomplished by using prominent four factors (slope, rainfall, geology, distance to thrust) which is more valid and reliable susceptibility model (Fig. 10).

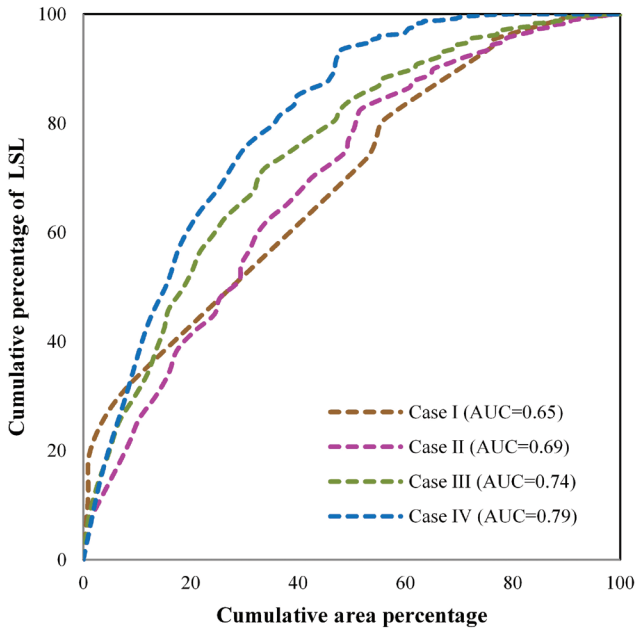

Fig. 10: Effect analysis of controlling factors for large-scale landslides (LSL).

CONCLUSIONS

The spatial distribution, failure characteristics of landslides and role of its controlling factors were examined from the datasets of small/large-scale landslides. The assessment of the landslide inventory with its controlling factors showed that slope geometry, landuse/land-cover, geology and proximity to river/road are the most influential controlling parameters for the spatial distribution of the landslides in the study area. The differential geological conditions associated with structural discontinuities, rainfall and slope geometry are the significant factors to control the LSL.

By crossing susceptibility and all landslides maps, it is found that 38.91%, 33.29% and 18.76% of landslides are overlaid in very high, high and medium susceptible zone; while around 9% of the landslides are located in low and very low susceptible zones. The result showed similar kind of distribution in case of LSL susceptibility zonation of 39.51%, 29.65% and 20.98% in very high, high and medium susceptible zones respectively.

The AUC of the success rates for all landslides is 0.67 whereas 0.58 for LSL from NFR model which is lower values in comparison to FR model 0.75 for all landslides and 0.69 is in LSL. Such a variation is attributed to the significance of the controlling factors in the case of large dimensional failures are due to complex mechanism which is clarifed from the effect analysis. Thus, the susceptibility model evaluations indicated that the major controlling factors for the LSL are the geology and structural discontinuities, slope geometry and rainfall with the predication accuracy of 79%.

ACKNOWLEDGEMENTS

This research study is supported by the University Grants Commission (UGC), Nepal as a PhD Support Grant, No. PhD-78/79-S&T-09. The authors are thankful to the two reviewers for their constructive comments for improving the manuscript.

REFERENCES

Baral, N., Karna, A. K., and Gautam, S., Landslide susceptibility assessment using modified frequency ration model in Kaski District, Nepal. International Journal of Engineering and Management Research, v. 11(1), pp. 167–177.

Bruckl, E. and Parotidis, M., 2001, Estimation of large-scale mechanical properties of a large landslide on the basis of seismic results. International Journal of Rock Mechanics and Mining Sciences, v. 38, pp. 877–883.

Bruckl, E., 2001, Cause-effect models of large landslides. Natural hazards, v. 23(2), pp. 291–314.

Cardenas, N. Y. and Mera, E. E., 2016, Landslide susceptibility analysis using remote sensing and GIS in the western Ecuadorian Andes. Natural Hazards, v. 81(3), pp. 1829–1859.

Carrara, A., Cardinali, M., Detti, R., Guzetti, F., Pasqui, V., and Reichenbach, P., 1991, GIS techniques and statistical models in evaluating landslide hazard. Earth Surface Processes and Landforms, v. 16, pp. 427–445.

Chalise, S. R. and Khanal, N. R., 2001, Rainfall and related natural disasters in Nepal. In: Tianchi, Li., Chalise, S. R., and Upreti, B. N. (eds.), Landslide hazards, mitigation to the Hindukush-Himalayas, ICIMOD, Kathmandu, pp. 63–70.

Chen, W., Chai, H., Sun, X., Wang, Q., Ding, X., and Hong, H., 2016, A GIS-based comparative study of frequency ratio, statistical index and weights-of-evidence models in landslide susceptibility mapping. Arabian Journal of Geosciences, v. 9(3), pp. 204.

Chen, Z., Liang, S., Ke, Y., Yang, Z., and Zhao, H., 2017, Landslide susceptibility assessment using evidential belief function, certainty factor and frequency ratio model at Baxie River Basin, NW China. Geocarto International.

Choi, J., Oh, H. J., Lee, H. J., Lee, C., and Lee, S., 2012, Combining landslide susceptibility maps obtained from frequency ratio, logistic regression, and artifcial neural network models using ASTER images and GIS. Engineering Geology, v. 124, pp.12–23.

Chung, C. F. and Fabbri, A. G., 1999, Probabilistic prediction models for landslide hazard mapping. Photogrammetric Engineering and Remote Sensing, v. 65, pp. 1389–1399.

Chung, C. F. and Fabbri, A., 2003, Validation of spatial prediction models for landslide hazard mapping. Natural Hazards, v. 30, pp. 451–472.

Chung, C. F., Fabbri, A. G., and Van Western, C. J., 1995, Multivariate regression analysis for landslide hazard zonation, In: Geographic Information Systems in Assessing Natural Hazards, Carrara, A. and Guzzetti, F. (Eds.), Kluwer, Dordrecht, pp. 107–133.

Chung, M., Chen, C., Lee, C., Huang, W., and Tan, C. 2018, Failure impact assessment for large-scale landslides located near human settlement: Case study in southern Taiwan. Sustainability, v. 10, pp. 1491.

Chung, M., Chen, C., Tan, C., Lee, C., and Huang, W., 2017, Investigation and assessment plan at the Xinzhuang potential large-scale landslide in southern Taiwan. World Landslide Forum, pp. 785–793.

Cruden, D. M. and Varnes, D. J., 1996, Landslide types and processes. In: Turner A. T., Schuster R. L. (Eds.) Landslides investigation and mitigation. Transportation Research Board Special Report no. 247. National Academy Press, Washington, DC, pp. 36–75.

Demir, G., Aytekin, M., Akgün, A., İkizler, S. B., and Tatar, O., 2013, A comparison of landslide susceptibility mapping of the eastern part of the North Anatolian Fault Zone (Turkey) by likelihood-frequency ratio and analytic hierarchy process methods. Natural Hazards, v. 65(3), pp. 1481–1506.

Devkota, K. C., Regmi, A. D., Pourghasemi, H. R., Yoshida, K., Pradhan, B., Ryu, I. C., Dhital, M. R., and Althuwaynee, O. F., 2013, Landslide susceptibility mapping using certainty factor, index of entropy and logistic regression models in GIS and their comparison at Muglin-Narayanghat road section in Nepal Himalaya. Natural Hazard, v. 65, pp. 135–165.

Dhital, M. R., 2015, Geology of the Nepal Himalaya: Regional Perspective of the Classic Collided Orogen. Springer International Publishing, Switzerland. In: Lesser Himalaya of Koshi Region, pp. 163–164.

Ding, Q., Chen, W., and Hong, H., 2017, Application of frequency ratio, weights of evidence and evidential belief function models in landslide susceptibility mapping. Geocarto International, v. 32(6), pp. 619–639.

DMG, 1980, Geological map of central Nepal. Department of Mines and Geology (DMG), Kathmandu, Nepal.

Dymond, J. R., Ausseil, A.G., Sheppard, J. D., and Buettner, L., 2006, Validation of a region-wide model of landslide susceptibility in the Manawatu-Wanganui region of New Zealand. Geomorphology, v. 74, pp. 70–79.

Fleuchaus, P., Blum, P., Wilde, M. Terhorst, B., and Butscher, C., 2021, Retrospective evaluation of landslide susceptibility maps and review of validation practice. Environmental Earth Sciences,

v. 80, pp. 485.

Ghobadi, M. H., Firuzi, M., and Noorzad, A., 2017, A large-scale landslide and related mechanism: a case study in the Qazvin-Rasht freeway, Iran. Environmental Earth Sciences, v. 76, pp. 478.

Giles, P. T. and Franklin, S. E., 1998, An automated approach to the classification of the slope units using digital data. Geomorphology, v. 21(3-4), pp. 251–264.

Gorsevski, P. V., Gessler, P., and Foltz, R. B., 2000, Spatial prediction of landslide hazard using discriminant analysis and GIS. In: GIS in the Rockies 2000 Conference and Workshop Applications for the 21st Century. Denver, Colorado. September 25–27, 2000.

Guzzetti, F., Carrara, A., Cardinali, M., and Reichenbach, P., 1999, Landslide hazard evaluation: a review of current techniques and their application in a multi-scale study, Central Italy. Geomorphology, v. 31, pp. 181–216.

Hasegawa, S., Dahal, R. K., Yamanaka, M., Bhandari, N. P., Yatabe, R., and Inagaki, H., 2008, Causes of large-scale landslides in the Lesser Himalaya of central Nepal. Environmental Geology, v. 57, pp. 1423–1434.

Hong, H., Pourghasemi, H. R., and Pourtaghi, Z. S., 2016, Landslide susceptibility assessment in Lianhua County (China): a comparison between a random forest data mining technique and bivariate and multivariate statistical models. Geomorphology, v. 259, pp. 105–118.

Huang, R. Q. and Li, W. L., 2008, Research on development and distribution rules of geohazards induced by Wenchuan earthquake on 12th May, 2008. Chinese Journal of Rock Mechanics and Engineering, v. 27(12), pp. 2585–2592. (In Chinese)

Huang, R. Q. and Li, W. L., 2009, Fault effect analysis of geo-hazard triggered by Wenchuan earthquake. Journal of Engineering Geology, v. 17(1), pp. 19–28. (In Chinese)

Hungr. O., leroueil, S., and Picarelli, L., 2014, The Varnes classification of landslide types, an update. Landslides. DOI: 10.1007/s10346-013-0436-y

IAEG Commission on Landslides, 1990, Suggested nomenclature for landslides. Bulletin of the international Association of Engineering Geology, v. 41, pp. 13–16.

Ilia, I. and Tsangaratos, P., 2016, Applying weight of evidence method and sensitivity analysis to produce a landslide susceptibility map. Landslides, v. 13, pp. 379–397.

Kuo, H. L., Lin, G. W., Chen, C. W., Saito, H., Lin, C. W., Chen, H., and Chao, W. A., 2018, Evaluating critical rainfall conditions for large-scale landslides by detecting event times from seismic records. Natural Hazards and Earth System Sciences, v. 18, pp. 2877–2891.

Lee, S. and Talib, J. A., 2005, Probabilistic landslide susceptibility and factor effect analysis. Environmental Geology, v. 47, pp. 982–990.

Lee, S., Choi, J., and Woo, I., 2004, The effect of spatial resolution on the accuracy of landslide susceptibility mapping: a case study in Boun, Korea. Geosciences Journal, v. 8, pp. 51–60.

Li, L., Xu, C., Yao, X., Shao, B., Ouyang, J., Zhang, Z., and Huang, Y., 2022, Large-scale landslides around the reservoir area of Baihetan hydropower station in Southwest China: Analysis of the spatial distribution. Natural Hazards Research, v. 2, pp. 218–229.

Lin, M., Chen, T., Lin, C., Ho, D., Cheng, K., Yin, H., and Chen, M., 2013, Detecting large-scale landslides using lidar data and aerial photos in the Namasha-Liuoguey area, Taiwan. Remote Sensing, v. 6, pp. 42–63.

Luzi, L. and Pergalani, F., 1996, A methodology for slope instability zonation using a probabilistic method. Actas VI Congreso Nacional y Conferensia Internasional de Geologia Ambiental y Ordencion del Territorio, v. 1, pp. 537–556.

Meusburger, K. and Alewell, C., 2009, On the influence of temporal change on the validity of landslide susceptibility maps. Natural Hazards and Earth System Sciences, v. 9(4), pp. 1495–1507.

Mohammady, M., Pourghasemi, H. R., and Pradhan, B., 2012, Landslide susceptibility mapping at Golestan Province, Iran: a comparison between frequency ratio, Dempster-Shafer, and weights-of-evidence models. Journal of Asian Earth Science, v. 61, pp. 221–236.

Mondal, S. and Maiti, R., 2013, Integrating the analytical hierarchy process (AHP) and the frequency ratio (FR) model in landslide susceptibility mapping of Shiv-khola watershed. International Journal of Disaster Risk Science, v. 4(4), pp. 200–212.

Moore, I. D., Grayson, R. B., and Ladson, A. R., 1991, Digital terrain modeling: A review of hydrological, geomorphological and biological applications. Hydrological Processes, v. 5, pp. 3–30.

Nepal, N., Chen, J., Chen, H., Wang, X., and Sharma T. P., 2019, Assessment of landslide susceptibility along the Araniko Highway in Poiqu/Bhote Koshi/Sun Koshi Watershed, Nepal Himalaya. Progress in Disaster Science, v. 3, pp. 1–10.

Pathak, D., 2016, Knowledge based landslide susceptibility mapping in the Himalayas. Geoenvironmental Disasters, v. 3(1), pp. 8.

Pellicani, R., Van Westen, C. J., and Spilotro, G., 2014, Assessing landslide exposure in areas with limited landslide information. Landslides, v. 11, pp. 463–480.

Pimiento, E., 2010, Shallow landslide susceptibility: modelling and validation. Dept. of Physical Geography and Ecosystem Science—Lund University. Thesis, pp. 25–29.

Pradhan, B. and Lee, S., 2010, Landslide susceptibility assessment and factor effect analysis: backpropagation artificial neural networks and their comparison with frequency ratio and bivariate logistic regression modelling. Environmental Modelling and Software, v. 25, pp. 745–759.

Regmi, A. D., Devkota, K. C., Yoshida, K., Pradhan, B., Pourghasemi, H. R., Kumamoto, T., and Akgun, A., 2012, Application of frequency ration, statistical index, and weights-of-evidence models and their comparison in landslide susceptibility mapping in Central Nepal Himalaya. Arabian Journal of Geosciences, v. 7, pp. 725–742.

Reis, S., Yalcin, A., Atasoy, M., Nisanci, R., Bayrak, T., Erduran, M., Sancar, C., and Ekercin, S., 2012. Remote sensing and GIS-based landslide susceptibility mapping using frequency ratio and analytical hierarchy methods in Rize province (NE Turkey). Environmental Earth Sciences, v. 66(7), pp. 2063–2073.

Riley, S., De Gloria, S. D., and Elliot, R., 1999, A terrain ruggedness index that quantifies topographic heterogeneity. Intermountain Journal of Sciences, v. 5(1-4), pp. 23–27.

Shang, Y., Yang, Z., Li, L., Liu, D., Liao, Q., and Wang, Y., 2003, A super large landslide in Tibet in 2000: background, occurrence, disaster, and origin. Engineering Geology, v. 54, pp. 225–243.

Shroder, J. F. and Bishop, M. P., 1998, Mass movement in the Himalaya: new insights and research directions. Geomorphology, v. 26, pp. 13–35.

Silalahi, F. E. S., Pamela, Arifianti Y., Hidayat, F., 2019, Landslide susceptibility assessment using frequency ratio model in Bogor, West Java, Indonesia. Geoscience. Lett. 6, 10. https://doi.org/10.1186/s40562-019-0140-4

Stöcklin, J. and Bhattarai, K. D., 1977, Geology of Kathmandu area

and central Mahabharat Range, Nepal Himalaya. HMG/UNDP mineral exploration project, Technical report, unpublished, pp. 86.

Stöcklin, J., 1980, Geology of Nepal and its regional frame. Journal of Geological Society of London, v. 137, pp. 1–34.

Thapa, P. B., 2011, Landslide susceptibility modelling in the central Nepal Lesser Himalaya. Jour. of Appl. Reg. Geol. (ZDGG), v. 162(4), pp. 405–420.

Timilsina, M., Bhandary, N. P., Dahal, R. K., and Yatabe, R., 2012, Typical morphometric and geological characteristics of large-scale landslides in central Nepal. Jour. Nepal Geol. Soc., v. 44, pp. 45–58.

Trigila, A., Ladanza, C., Munafo, M., and Marinosci, I., Population exposed to landslide and flood risk in Italy. Engineering Geologu for Society and Territory, v. 3, pp. 843–848.

Umar, Z., Pradhan, B., Ahmad, A., Jebur, M. N., and Tehrany, M. S., 2014. Earthquake induced landslide susceptibility mapping using an integrated ensemble frequency ratio and logistic regression models in West Sumatera Province, Indonesia. CATENA, v. 118, pp. 124–135.

Van Western, C. J., Castellanos, E., and Kuriakose, S. L., Spatial data for landslide susceptibility, hazard, and vulnerability assessment: An overview. Engineering Geology, v. 102(3-4), pp. 112–131.

Varnes, D. J., 1978, Slope movement types and processes. In: Schuster, R. L. and Krizek, R. J. (eds.), Special Report 176: Landslides: Analysis and Control. Transportation and Road Research Board, National Academy of Science, Washington D. C., pp. 11–33.

Wahono, B. F. D., 2010, Applications of statistical and heuristic methods for land- slide susceptibility assessments, a case study in Wadas Lintang Sub District, Wonosobo Regency, Central Java Province, Indonesia. GeoInforma- tion for Spatial Planning and Risk Management Jogjakarta—Enschede, Gadjah Mada—ITC. Thesis, pp. 12–37.

Wang, Q. and Li, W., 2017, A GIS-based comparative evaluation of analytical hierarchy process and frequency ratio models for landslide susceptibility mapping. Physical Geography, v. 38(4), pp. 318–337.

Wen, B. and Chen, H., 2007, Mineral compositions and elements concentrations as indicators for the role of groundwater in the development of landslide slip zones: a case study of large-scale landslides in the Three Gorges Area in China. Earth Science Frontiers, v. 14(6), pp. 98–106.

Wilson, A. J., Petley, D. N., and Murphy, W., 2003, Down-slope variation in geotechnical parameters and pore fluid control on a large-scale Alpine landslide. Geomorphology, v. 54, pp. 49–62.

WP/WLI, 1993, A suggested method for describing the activity of a landslide. Bulletin of the international Association of Engineering Geology, v. 47, pp. 53–57.

Wubalem, A., 2021, Landslide susceptibility mapping using statistical methods in Uatzau catchment area, northwestern Ethiopia. Geoenvironmental Disasters, v. 8, pp. 1. https://doi.org/10.1186/s40677-020-00170-y

Xu, Q., Zhang, S., and Li, W., 2011, Spatial distribution of large-scale landslides induced by the 5.12 wenchuan earthquake. Journal of Mountain Sciences, v. 8, pp. 246–260.

Yalcin, A., Reis, S., Aydinoglu, A. C., and Yomralioglu, T., 2011, A GIS-based comparative study of frequency ratio, analytical hierarchy process, bivariate statistics and logistics regression methods for landslide susceptibility mapping in Trabzon, NE Turkey. Catena, v. 85, pp. 274–287.

Youssef, A. M., Pradhan, B., Pourghasemi, R. H., and Abdullahi, S., Landslide susceptibility assessment at Wadi Jawrah Basin, Jizan region, Saudi Arabia using two bivariate models in GIS. Geosciences Journal, v. 19, pp. 449–469.

Zerathe, S., Lebourg, T., Braucher, R., and Bourles, D., 2014, Mid-Holocene cluster of large-scale landslides revealed in the Southwestern Alps by 36CI dating. Insight on an Alpine-scale landslide activity. Quaternary Science Reviews, v. 90, pp. 106–127.

Zhao, B., Wang, Y., Luo, Y., Liang, R., Li, J., and Xie, L., 2019, Large landslides at the northeastern margin of the Bayan Har Block, Tibetan Plateau, China. Royal Society open science, v. 6(180844). DOI: 10.1098/rsos.180844

Zhou, X. P. and Cheng, H., 2015, The long-term stability analysis of 3D creeping slopes using the displacement-based rigorous limit equilibrium method. Engineering Geology, v. 195, pp. 292–300.